Hindawi
Shock and Vibration
Volume 2021, Article ID 6626715, 9 pages
https://doi.org/10.1155/2021/6626715

Research Article

Numerical Simulation and Experimental Study on Flow Field in a Swirl Nozzle

Yicheng Sun,[1] Yufan Fu ,[2,3] Baohui Chen,[1] Jiaxing Lu,[2,3] and Wanquan Deng[2,3]

[1]*State Grid Hunan Electric Power Co., Ltd. Disaster Prevention and Mitigation Center State Key Laboratory of Disaster Prevention and Mitigation for Grid Transmission and Distribution Equipment, Changsha 410015, China*
[2]*Key Laboratory of Fluid and Power Machinery Ministry of Education, Xi Hua University, Chengdu 610039, China*
[3]*School of Energy and Power Engineering, Xi Hua University, Chengdu 610039, China*

Correspondence should be addressed to Yufan Fu; 729203966@qq.com

Received 25 November 2020; Revised 1 January 2021; Accepted 15 January 2021; Published 27 January 2021

Academic Editor: Ling Zhou; lingzhou@ujs.edu.cn

In order to study the internal flow characteristics and external droplet velocity distribution characteristics of the swirl nozzle, the following methods were used: numerical simulations were used to study the internal flow characteristics of a swirl nozzle and phase Doppler particle velocimetry was used to determine the corresponding external droplet velocity distribution under medium and low pressure conditions. The distributions of pressure and water velocity inside the nozzle were obtained. Meanwhile, the velocities of droplets outside the nozzle in different sections were discussed. The results show that the flow rate in the swirl nozzle increases with the increase in inlet pressure, and the local pressure in the region decreases because of the excessive velocity at the internal outlet section of the swirl nozzle, resulting in cavitation. The experimental results show that under an external flow field, the minimum droplet velocity occurs in the axial direction; starting from the axis, the velocity first increases and then decreases along the radial direction. Swirling motion inside the nozzle and velocity variations in the external flow field occur under medium and low pressure conditions. The relationship between the inlet pressure and the distributions of water droplets' velocities was established, which provides a reference for the research and development of the swirl nozzle.

1. Introduction

Water-mist fire extinguishing technology is playing an increasingly important role in the field of modern fire protection. Water is the main medium employed by this technology, where a pressurized water mist is sprayed to extinguish a fire at the source [1, 2]. Pressure nozzles are widely used in fire protection because of their simple structure, large atomization angle, and production of a uniform droplet distribution [3].

Studies on the structural design of a water mist fire extinguishing nozzle have been carried out. Du et al. [4, 5] designed a novel nozzle structure to improve atomization. Bhattacharya and Hu investigated the atomization characteristics of the water mist used to extinguish fires; experiments were conducted on the spray characteristics of pressure atomization nozzles, and the intensity of spray was reported to significantly impact fire extinguishing [6, 7]. Marchione et al. [8–10] studied spray characteristics, such as the spray cone angle and the film breakage length, of the external flow field under different spray pressures. Jedelsky et al. [11, 12] studied the formation of a hollow cone spray and the chang law of the spray cone angle. Xia et al. [13] studied spray characteristics and found that the breaking length of the water jet decreases as the gas-liquid ratio in the air increases. Mayer and Branam [14] studied the characteristic parameters of a water-mist fog field under different pressure conditions and found that the intensity distribution of the water mist flow field narrowed as the pressure increased. Wu et al. [15, 16] found that the fog cone angle increased with the increase in the discharge coefficient. Wang et al. [17, 18] used

numerical simulations to investigate the flow mechanism of atomizing nozzles.

However, few studies have been conducted to determine the characteristics of the internal flow in swirl nozzles and the external droplet velocity distribution. Therefore, in order to provide more research and corresponding data for reference, the characteristics of the internal flow field and the external droplet velocity distribution of a swirl nozzle are investigated in this study under medium and low pressure conditions; the internal flow profile in the swirl nozzle and the change law of the external droplet velocity are presented.

2. Numerical Simulation of Swirl Nozzle

2.1. Geometric Model and Meshing. The object of this study is a straight-blade swirl nozzle. The two-dimensional nozzle structure is shown in Figure 1. The nozzle inlet diameter D_1 is 14 mm, the outlet diameter D_2 is 6 mm, L_1 is the jet exit section, and L is the total nozzle, in which water flows through. After the two symmetrical straight blades collide with each other to form a swirling flow, water shoots out the nozzle exit section.

Figure 2 shows the three-dimensional structure of the nozzle and the three-dimensional water body in the nozzle (which is meshed by ICEM). The total number of grids shown in Figure 3 is 842088.

2.2. Parameter Settings. This study uses Fluent software for double-precision numerical calculation. The inlet pressure of the swirl nozzle is set to 1 MPa, 2 MPa, 3 MPa, 4 MPa, 5 MPa, and 6 MPa, the outlet pressure is one atmosphere, the reference pressure is 0 Pa, and the wall surface is a nonslip boundary. The phase flow model uses the Euler-Euler two-fluid model, the turbulence model is the standard $k-\varepsilon$ model, and the pressure-velocity coupling uses the SIMPLEC algorithm.

2.3. Calculation Model

2.3.1. Turbulence Model. The water flow inside the water mist nozzle becomes unstable under turbulence. The standard $k-\varepsilon$ model [19–24] application is currently the most commonly used turbulence model. This model has high calculation accuracy and good stability and is therefore used for numerical calculations in this study.

The standard $k-\varepsilon$ model equation is given as follows:

k transport equation is as follows:

$$\frac{\partial \rho k}{\partial t}+\frac{\partial (\rho k u_i)}{\partial x_i}=\frac{\partial}{\partial_{x_i}}\left[\left(\mu+\frac{\mu_i}{\sigma_k}\right)\frac{\partial k}{\partial x_j}\right]+G_k+G_b - \rho\varepsilon - Y_M+S_k. \tag{1}$$

ε transport equation is as follows:

$$\frac{\partial (\rho\varepsilon)}{\partial t}+\frac{\partial (\rho\varepsilon u_i)}{\partial x_i}=\frac{\partial}{\partial x_i}\left[\left(\mu+\frac{\mu_i}{\sigma_\varepsilon}\right)\frac{\partial \varepsilon}{\partial x_j}\right] + C_{1\varepsilon}\frac{\varepsilon}{k}\left(G_k+C_{3\varepsilon}G_b\right)-C_{2\varepsilon}\rho\frac{\varepsilon^2}{k}+S_t, \tag{2}$$

where G_k represents the effect of the velocity gradient on the turbulent kinetic energy k (kg/(m·s^3)), G_b denotes the production of turbulent kinetic energy k caused by buoyancy (kg/(m·s^3)), Y_M represents pulsation expansion in compressible turbulence (kg/(m·s^3)), $C_{1\varepsilon}$, $C_{2\varepsilon}$, and $C_{3\varepsilon}$ are empirical constants, and S_k and S_t are user-defined source terms (kg/(m·s^3)), and $C_{1\varepsilon}=1.44$, $C_{2\varepsilon}=1.92$, $C_{3\varepsilon}=0.09$, $\sigma_k=1.0$, and $\sigma_\varepsilon=1.3$.

2.3.2. Multiphase Flow Model. The Euler-Euler two-fluid model [25–30] established a set of n momentum equations and continuity equations that are solved for each phase. This model has the advantage of fully considering turbulent transport of the particle phase, unlike the Euler–Lagrange method; the Euler-Euler two-fluid model assumes that the discrete droplet phase is a pseudo-fluid, which requires low computation. Therefore, the Euler-Euler two-fluid model is used in this study to numerically simulate the internal flow field of the swirl nozzle. The flow is treated as incompressible, and the governing equations are given as follows:

Continuity equation of the kth phase is as follows:

$$\frac{\partial}{\partial t}\left(\alpha_k\rho_k\right)+\nabla\cdot\left(\alpha_k\rho_k\overrightarrow{v_k}\right)=0. \tag{3}$$

Momentum conservation equation of the kth phase is as follows:

$$\frac{\partial}{\partial t}\left(\alpha_k\rho_k u_k\right)+\nabla\cdot\left(\alpha_k\rho_k\overrightarrow{v_k}\,\overrightarrow{u_k}\right)=m_{pk}u_{pk}+\nabla\cdot\overrightarrow{\tau_k} - \alpha_k\left(\nabla p-\rho_k F_L-\rho_k F_{Vm}-\rho_k F_k\right)+\overrightarrow{R}_{pq}, \tag{4}$$

where∇ is the divergence; m_{pk} is the quality of k-phase, kg; v is the gas flow velocity of k-phase, m/s; α_k is the volume fraction of the k th phase, %; τ_k is the shear stress of the k th phase; p is the pressure, Pa; F_L and F_{Vm} are the lift and virtual mass force, respectively, N; and $\overline{R}_{pq}$ is the interphase force between the phase volumes, where $\overline{R}_{pq}=-\overline{R}_{pq}$ and $\overline{R}_{pq}=0$. The volume fraction is defined as the space occupied by each phase, where each phase satisfies the law of conservation of mass and momentum. The volume fraction is denoted by α_k. The volume V_k of phase k is defined as $V_k=\int\alpha_k dV$, where the sum of the phases of α_k is 1.

2.4. Analysis of Numerical Simulation Results

2.4.1. Pressure Distribution in Swirl Nozzle under Different Inlet Pressures. Figure 4 shows the numerical simulation results for the swirl nozzle pressure distribution at the center

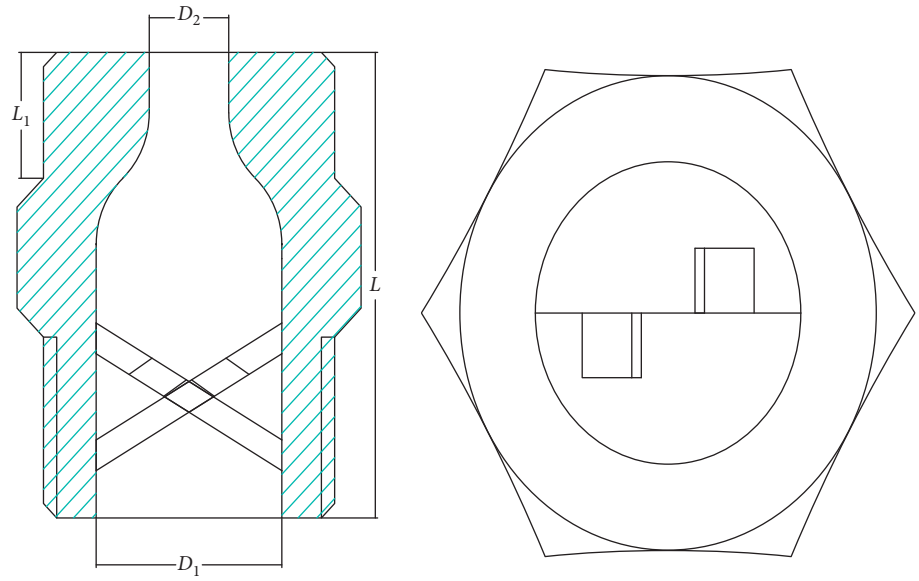

Figure 1: Diagram of swirl nozzle structure.

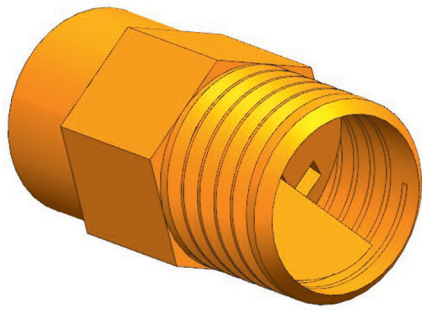

Figure 2: Space model of the swirl nozzle.

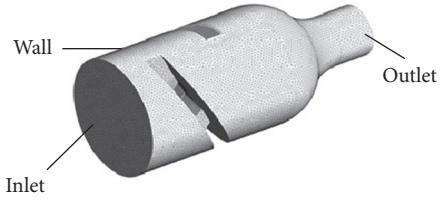

Figure 3: Calculation model of the swirl nozzle.

section ($Z = 0$) of the nozzle under different inlet pressure conditions. The inlet pressure of the swirl nozzle is set to 1 MPa, 2 MPa, 3 MPa, 4 MPa, 5 MPa, and 6 MPa from small to large.

Water flows through the straight blades to form a swirling flow in the nozzle chamber and then shoots out the nozzle. Figure 4 shows that for inlet pressures of 1 MPa and 6 MPa, the negative pressure at the center section of the swirl nozzle outlet is 0.29 MPa and 1.59 MPa. As the inlet pressure of the swirl nozzle increases, the local pressure at the outlet section gradually decreases, which causes the velocity of the center point of the jet to be lower than the velocity at other areas after the jet exits from the nozzle.

2.4.2. Velocity Distribution of Swirl Nozzles under Different Pressures. The velocity distribution at the center section of the swirl nozzle is shown in Figure 5. The water velocity in the nozzle increases with the inlet pressure. For inlet pressures of 1 MPa and 6 MPa, the maximum velocity at the outlet section is 39.23 m/s and 96.35 m/s. Comparing Figures 4 and 5 shows that the maximum in the speed distribution of the speed cloud chart occurs in the low pressure area.

2.4.3. Streamline Distribution of Outlet Section under Different Inlet Pressures. Figure 6 shows the velocity distribution at the outlet section under different nozzle inlet pressures. The low pressure zone at the center of the nozzle outlet causes the water jet to be ejected from the edge at a high speed. Figure 6 shows that under different inlet pressure conditions, as the radial direction displacement increases, the speed gradually increases from the axis and then decreases rapidly near the edge of the section.

2.5. Test System and Measurement Method. The test system for the external flow field of the swirl nozzle is shown in Figure 7. The system has two main components, an atomization pipe spray system, which is composed of a water supply tank, valve, water pump, nozzle, water collecting tank, and connection pipe, and a test measurement system, which includes pressure sensor, an electromagnetic flowmeter, a phase Doppler velocimeter, particle size analyzer, and a computer. The velocity distribution of the external

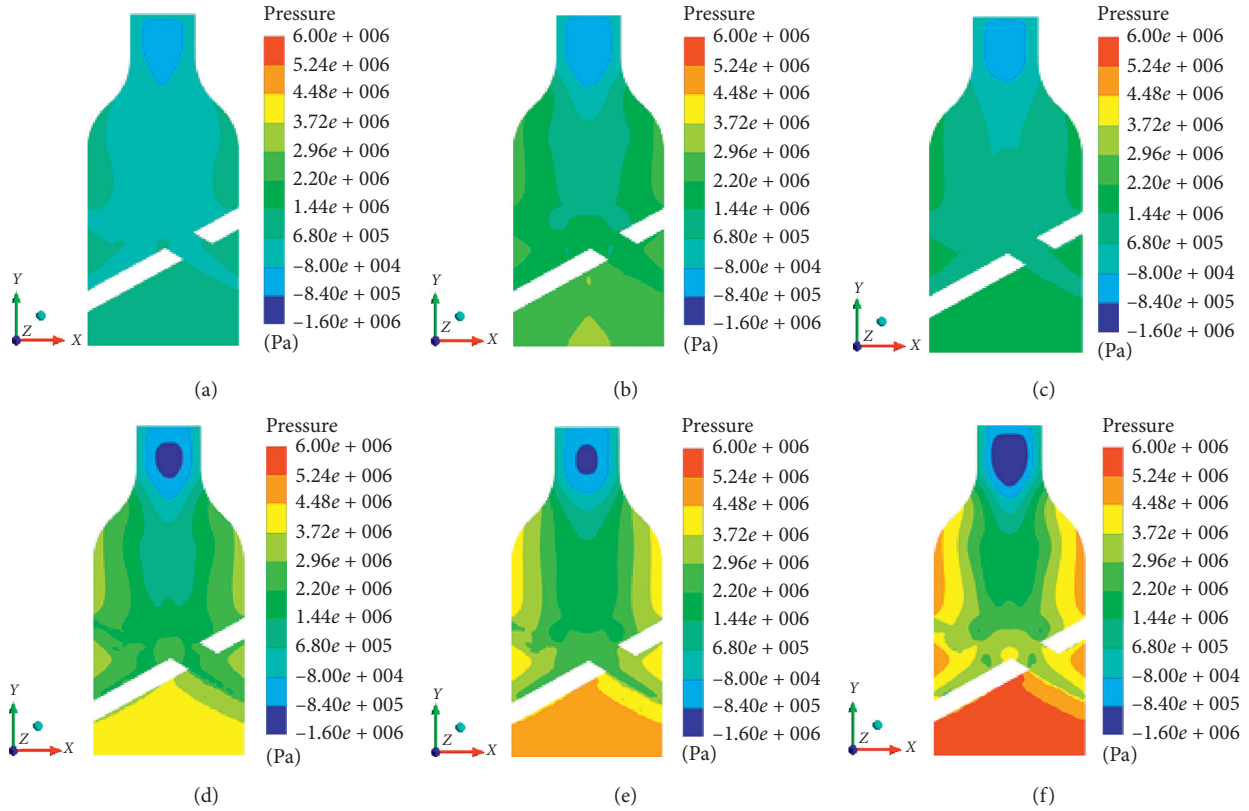

Figure 4: Pressure distribution in the central section of the swirl nozzle: (a) 1 MPa, (b) 2 MPa, (c) 3 MPa, (d) 4 MPa, (e) 5 MPa, and (f) 6 MPa.

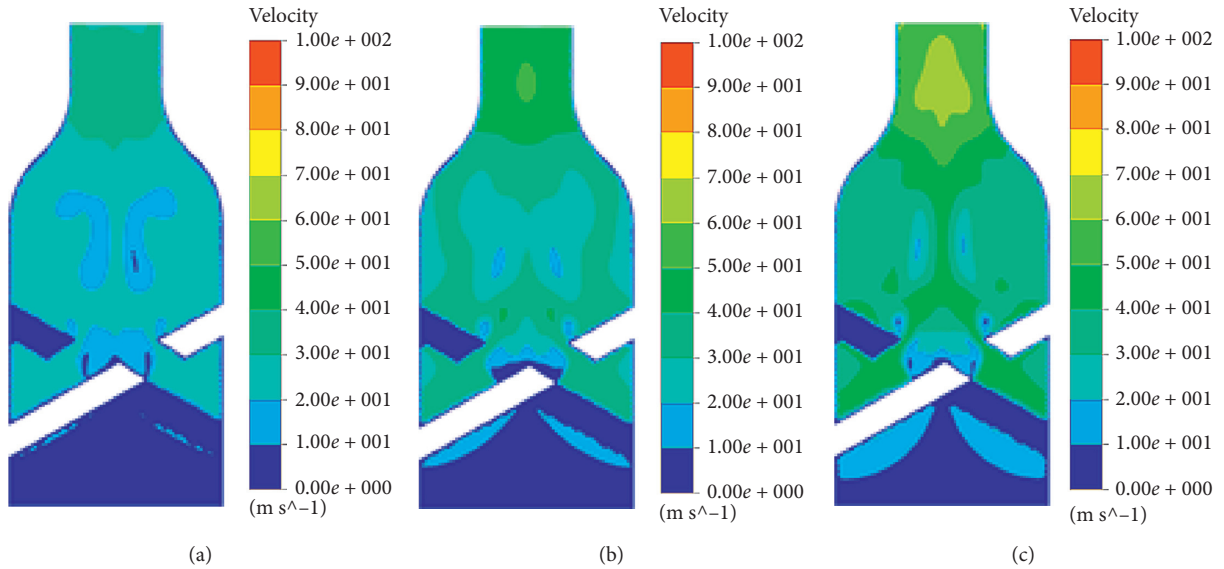

Figure 5: Continued.

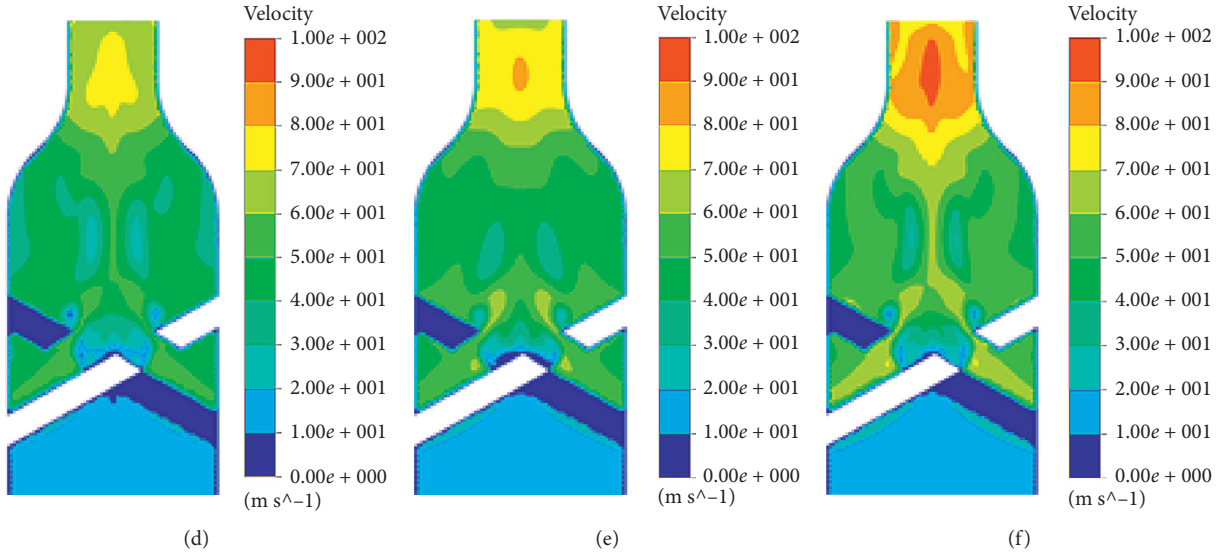

Figure 5: Velocity distribution in the center section of the swirl nozzle: (a) 1 MPa, (b) 2 MPa, (c) 3 MPa, (d) 4 MPa, (e) 5 MPa, and (f) 6 MPa.

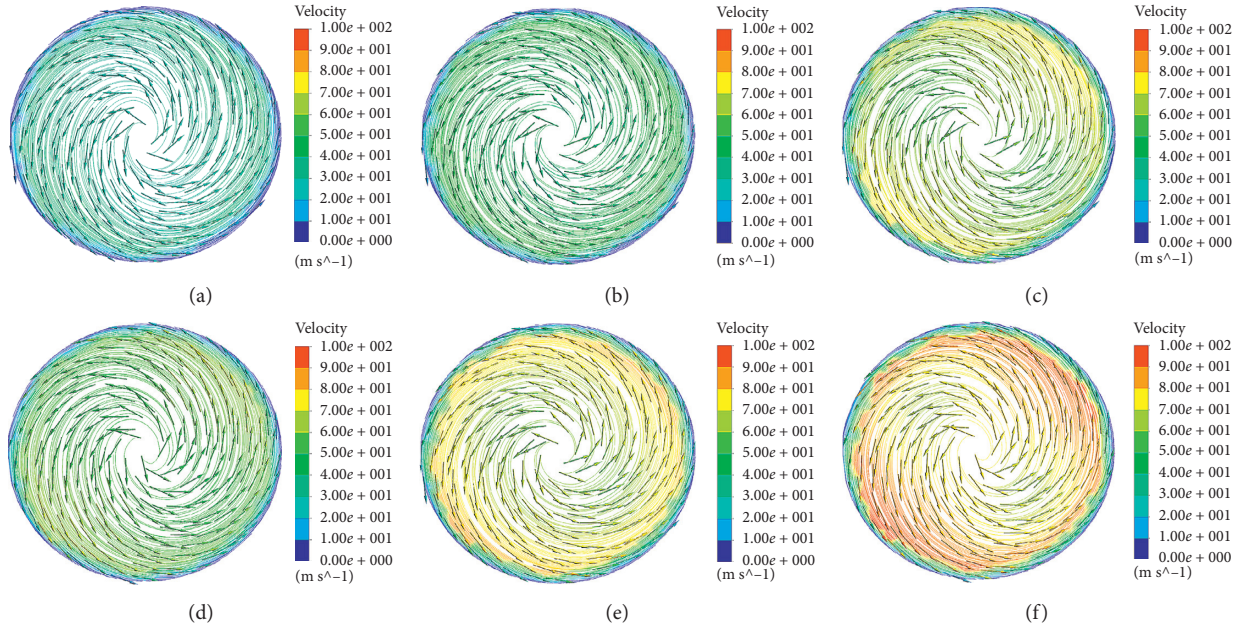

Figure 6: Streamline distribution in the center section of swirl outlet: (a) 1 MPa, (b) 2 MPa, (c) 3 MPa, (d) 4 MPa, (e) 5 MPa, and (f) 6 MPa.

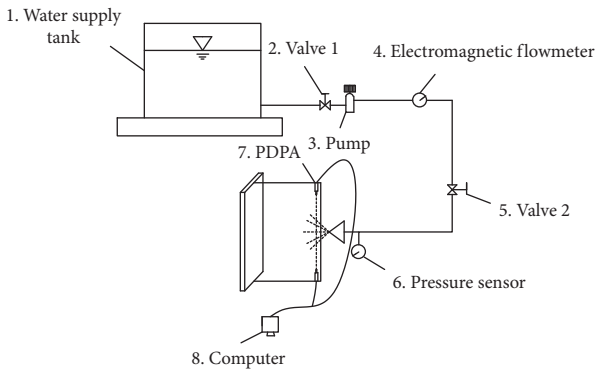

Figure 7: Diagram of the atomizing nozzle test system.

flow field of droplets is measured under different nozzle inlet pressures during the test.

The water tank is filled, and the water is sent to the test nozzle by adjusting valve 1 through the connecting pipe. After the test system is stable, the water pump test is formally started. The pressure sensor displays the water flow pressure; valve 2 is adjusted incrementally to increase the nozzle pressure to 1 MPa, 2 MPa, 3 MPa, 4 MPa, 5 MPa, and 6 MPa; the flow is read from the electromagnetic flowmeter; information from the phase Doppler velocimeter and particle size analyzer are processed using Flowersizer computer software and output as the velocity distribution of the droplets in the fog field. The test site is shown in Figure 8.

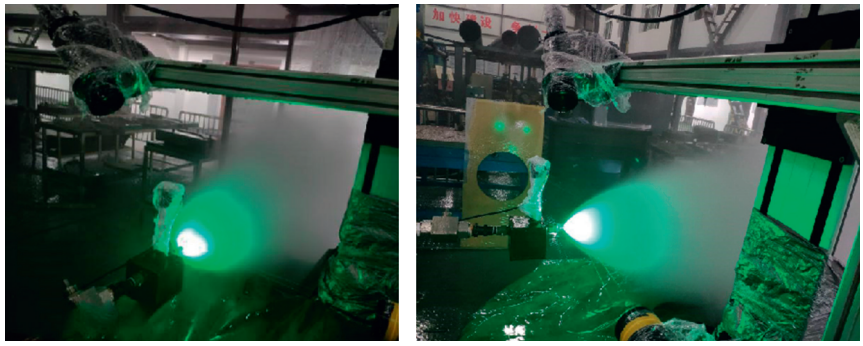

Figure 8: Test site.

Figure 9: Photograph of the atomizing nozzle.

3. Analysis of Test Results

3.1. Pressure-Flow Analysis. A photograph of the nozzle used in this study is shown in Figure 9. The nozzle is placed 1.5 m above ground. The measured nozzle inlet pressure and the flow rate through the nozzle are used to produce the pressure-flow curve, shown in Figure 10.

The initial pressure of the atomizing nozzle is 1 MPa. The flow rate increases approximately linearly with the inlet pressure, showing that indicates that increasing the inlet pressure increases the swirling motion of the water flow in the nozzle.

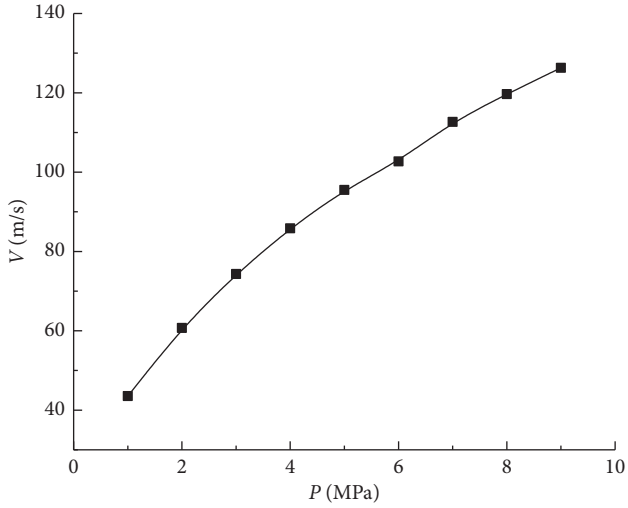

Figure 10: Characteristic pressure-flow curve.

3.2. Velocity Distribution of Particles in Fog Field. A field test is conducted to determine the external flow field of the nozzle, a straight-blade swirl nozzle is fixed on the bracket, and the pressure is adjusted to 2 MPa, 3 MPa, and 4 MPa for the test. Phase Doppler velocimetry measurement technology is used to determine the velocity at four cross-sections. Figure 11 shows the axial test sections of the nozzle at 20 mm, 30 mm, 40 mm, and 50 mm.

Figure 12 shows the variation in the radial velocity or Section 1 at a distance of 20 mm from the nozzle axial outlet. In the swirling nozzle, water flow through the swirling chamber produces a jet that is ejected from the nozzle in a rotating form and breaks into droplets in the surrounding air. For nozzle inlet pressures of 2 MPa and 3 MPa, the minimum speed is 28 m/s and 31.9 m/s, respectively. For an inlet pressure of 4 MPa, the minimum speed is 35.6 m/s. The droplet velocity gradually increases with the radial distance and reaches a maximum at 10 mm from the axial center. The maximum velocity is 43.2 m/s, 45.9 m/s, and 51.2 m/s for inlet pressures of 2 MPa, 3 MPa, and 4 MPa, respectively.

Figure 12 shows that the smallest droplet velocity occurs along the axis of the swirl nozzle. At the same cross-section, as the radial distance increases, the velocity first increases

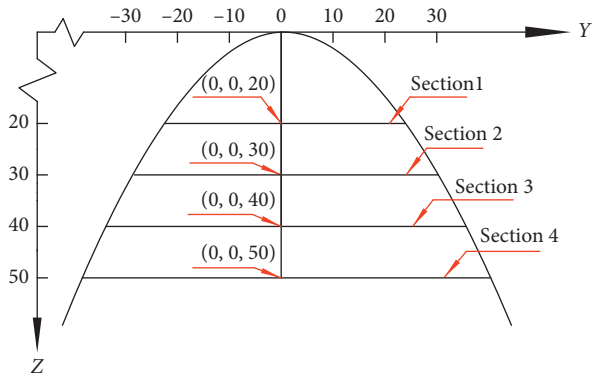

Figure 11: Test section.

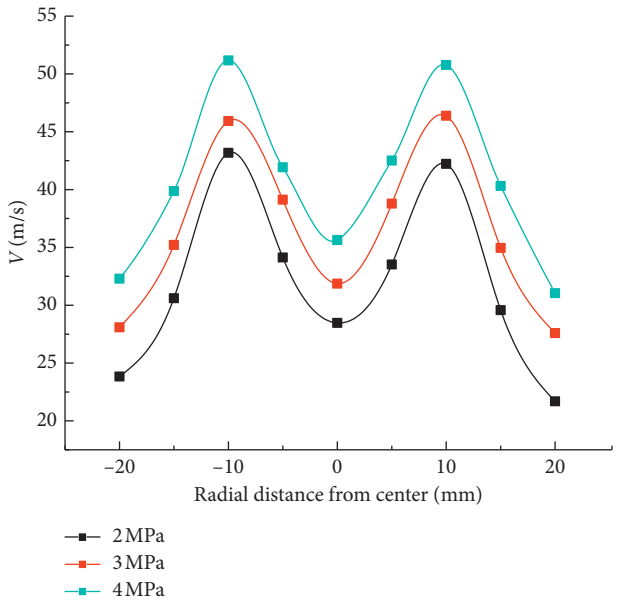

Figure 12: Radial velocity curve of Section 1.

from the axis and then decreases. This behavior is caused by cavitation from the low local pressure in the outlet section of the nozzle.

Figure 13 shows the variation in the radial velocity or Section 2 at a distance of 30 mm from the nozzle axial outlet. For inlet pressures 2 MPa, 3 MPa, and 4 MPa, the minimum axial speed is 22.3 m/s, 33.2 m/s, and 36.5 m/s, respectively. For an inlet pressure of 2 MPa, the maximum speed of 49 m/s occurs at 10 mm along the radial direction for Section 2. For an inlet pressure of 3 MPa, the maximum speed of 52.8 m/s occurs at 15 mm along the radial direction for Section 2. For an inlet pressure of 4 MPa, the maximum speed of 59 m/s occurs at 17 mm along the radial direction for Section 2. Figure 13 shows that the radial speed curve is approximately "M-shaped."

The variation in the radial velocity or Section 3 at 40 mm from the nozzle outlet is shown in Figure 14. At the axis, the minimum speed for the swirl nozzle is 24.1 m/s, 29.7 m/s, and 35.4 m/s for inlet pressures of 2 MPa, 3 MPa, and 4 MPa, respectively. In Section 3, the droplet velocity of the external

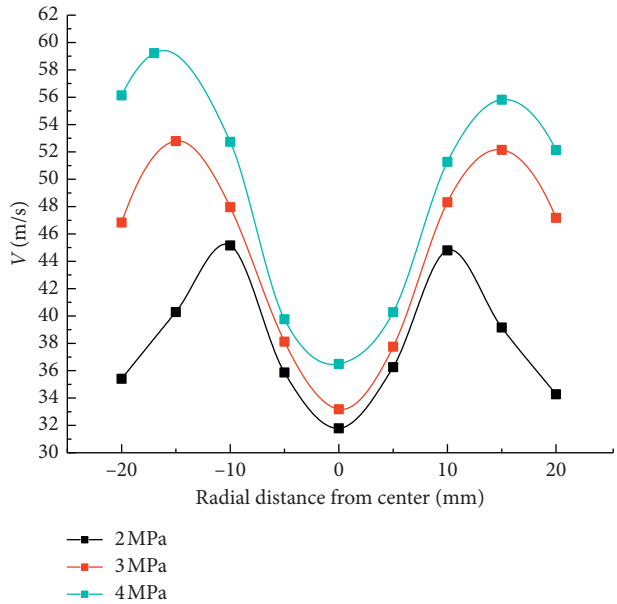

Figure 13: Radial velocity curve of Section 2.

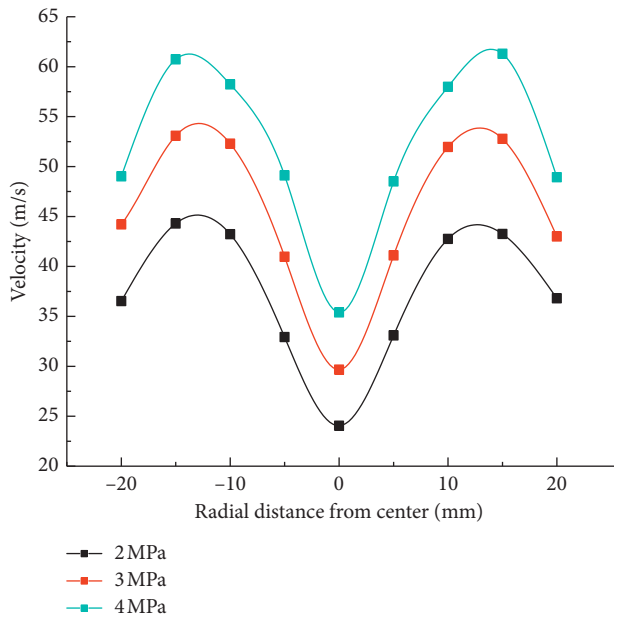

Figure 14: Radial velocity curve of Section 3.

flow field gradually increases along the radial direction and reaches a maximum at 15 mm. The maximum velocity is 44.3 m/s and 53.1 m/s for inlet pressures of 2 MPa and 3 MPa, respectively. For an inlet pressure of 4 MPa, the maximum speed is 60.7 m/s.

Figure 15 shows the variation in the radial velocity or Section 4 at a distance of 50 mm from the nozzle axial outlet. At the axis, the minimum speed in the nozzle is 25.0 m/s, 33.2 m/s, and 39.5 m/s for inlet pressures of 2 MPa, 3 MPa, and 4 MPa, respectively. The speed along the radial direction

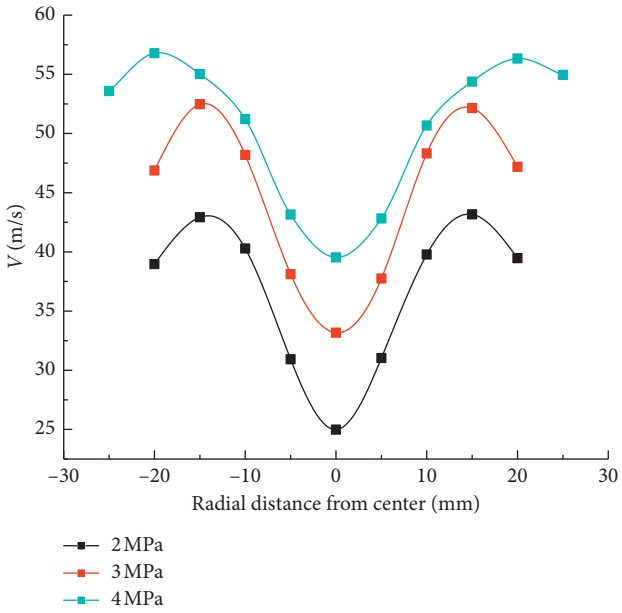

Figure 15: Radial velocity curve of Section 4.

for Section 4 reaches a maximum at 15 mm. The maximum speed is 42.9 m/s, 52.5 m/s, and 56.8 m/s for inlet pressures of 2 MPa, 3 MPa, and 4 MPa, respectively.

The experimental results show the same change trend in the velocity along the radial direction for different sections of the nozzle outlet. The smallest velocity occurs at the axis of the nozzle outlet. The speed of displacement increases rapidly to a maximum and decreases rapidly near the edge of the jet; under different nozzle inlet pressures, the speed reaches a maximum between 10 mm and approximately 15 mm and then rapidly decreases. These results are consistent with the conclusion of numerical simulation.

4. Conclusion

In this paper, numerical simulation and experimental study on the swirl nozzle are carried out. The results show that the speed and flow rate of water in a swirling nozzle increase gradually with the increase in pressure, which conforms to the general law of motion or a nozzle jet. As the inlet pressure of the swirl nozzle is gradually increased, an excessive velocity at the outlet section inside the nozzle causes a gradual decrease in the pressure at the outlet center. The results of experiments and numerical simulations show that the variation in the velocity in the swirl nozzle is caused by cavitation at the outlet center induced by low pressure. The smallest velocity for the external flow field occurs along the axial direction, and as the displacement in the radial direction of the external flow field increases, the velocity gradually increases starting from the axis and then decreases rapidly near the radial edge.

Data Availability

The data used to support the findings of this study are available from the #2 author (Yufan Fu) upon request.

Conflicts of Interest

The authors declare that they have no conflicts of interest.

Authors' Contributions

Y.S. (engineer) conceptualized the study and analyzed the data; B.C. (engineer) analyzed the data; Y.F. (master) engaged in water conservancy projects; J.L. (lecturer) engaged in hydraulic machinery research; W.D. (lecturer) engaged in fluid machinery testing technology experiments for long term, using PIV and LDV to carry out multiphase flow research.

Acknowledgments

This research was funded by the Major projects of State Grid Corporation of China (grant nos. 5216A0180006 and 5216A019000M) and the National Natural Science Foundation (grant no. 52009115) and the research on Wind-Resistant Medium Pressure Water Mist Nozzle (grant no. RH1900007925).

References

[1] A. Nasser, *Handbook of Atomization and Sprays*, Springer, Cambridge, MA, USA, 2011.

[2] Q. Y. Liu, X. Y. Yi, and Z. H. Lv, "Research progress of water mist fire extinguishing effectiveness," *Science Technology and Engineering*, vol. 19, no. 22, pp. 11–19, 2019.

[3] J. L. Santolaya, J. A. García, E. Calvo, and L. M. Cerecedo, "Effects of droplet collision phenomena on the development of pressure swirl sprays," *International Journal of Multiphase Flow*, vol. 56, pp. 160–171, 2013.

[4] Y. W. Du, Y. Guo, and A. X. Cao, "Design of direct-injection-swirl premixed water mist nozzle and experimental research on oil fire suppression," *Fire Science and Technology*, vol. 38, no. 06, pp. 827–832, 2019.

[5] D. Hua, Q. G. Li, and B. Tang, "Design of multi-nozzle combined direct swirling water mist fire extinguishing nozzle," *Journal of Xihua University*, vol. 34, no. 02, pp. 108–112, 2015.

[6] P. Bhattacharya, A. N. Samanta, and S. Chakraborty, "Spray evaporative cooling to achieve ultra fast cooling in runout table," *International Journal of Thermal Sciences*, vol. 48, no. 9, pp. 1741–1747, 2009.

[7] C. P. Hu, X. Que, and L. Su, "The application research of low pressure water mist for use in category machinery spaces," *Fire Science and Technology*, vol. 3, pp. 311–313, 2005.

[8] T. Marchione, C. Allouis, and A. Amoresano, "Experimental investigation of a pressure swirl atomizer spray," *Journal of Propulsion & Power*, vol. 23, no. 05, pp. 1096–1101, 2012.

[9] M. Rashad, H. Yong, and Z. Zekun, "Effect of geometric parameters on spray characteristics of pressure swirl atomizers," *International Journal of Hydrogen Energy*, vol. 41, no. 35, pp. 15790–15799, 2016.

[10] M. Rashid, A. H. A. Hamid, and O. Sheng, "Effect of inlet slot number on the spray cone angle and discharge coefficient of swirl atomize," *Procedia Engineering*, vol. 56, pp. 160–171, 2012.

[11] J. Jedelsky, M. Maly, N. Pinto del Corral, G. Wigley, L. Janackova, and M. Jicha, "Air-liquid interactions in a

pressure-swirl spray," *International Journal of Heat and Mass Transfer*, vol. 121, pp. 788–804, 2018.

[12] J. L. Santolaya, L. A. Aísa, E. Calvo, I. García, and J. A. García, "Analysis by droplet size classes of the liquid flow structure in a pressure swirl hollow cone spray," *Chemical Engineering and Processing: Process Intensification*, vol. 49, no. 1, pp. 125–131, 2010.

[13] Y. Xia, M. Alshehhi, Y. Hardalupas, and L. Khezzar, "Spray characteristics of free air-on-water impinging jets," *International Journal of Multiphase Flow*, vol. 100, pp. 86–103, 2018.

[14] W. O. H. Mayer and R. Branam, "Atomization characteristics on the surface of a round liquid jet," *Experiments in Fluids*, vol. 36, no. 04, pp. 528–539, 2004.

[15] Y. Wu, L. Lu, and S. H. Feng, "The relationship between the discharge coefficient of the high-pressure water mist nozzle and the characteristics of the fog field," *Science Technology and Engineering*, vol. 18, no. 01, pp. 348–352, 2018.

[16] M. R. Halder, S. K. Dash, and S. K. Som, "A numerical and experimental investigation on the coefficients of discharge and the spray cone angle of a solid cone swirl nozzle," *Experimental Thermal and Fluid Science*, vol. 28, no. 4, pp. 297–305, 2004.

[17] J. Wang, Z. W. Gao, and X. M. Zhang, "Study on the characteristics of gas-liquid two-phase flow in swirl atomization nozzle," *Petroleum Refining and Chemical Industry*, vol. 51, no. 03, pp. 54–61, 2020.

[18] B. C. Wang, K. Zhang, and D. Zhang, "Simulation of supersonic gas-liquid mixing nozzle based on fluent," *Clean the World*, vol. 36, no. 01, pp. 35–37, 2020.

[19] X. X. Li and Q. T. Eri, "Investigation of infrared radiation characteristic of axisymmetric exhaust system using variable diffusion turbulence model," *Journal of Propulsion and Technology*, vol. 34, no. 03, pp. 289–293, 2013.

[20] X. Li, T. Shen, and P. Li, "Extended compressible thermal cavitation model for the numerical simulation of cryogenic cavitating flow," *International Journal of Hydrogen Energy*, vol. 45, no. 16, 2020.

[21] L. Bai, L. Zhou, X. Jiang, Q. Pang, and D. Ye, "Vibration in a multistage centrifugal pump under varied conditions," *Shock and Vibration*, vol. 2019, pp. 1–9, Article ID 2057031, 2019.

[22] S. Tang, S. Yuan, and Y. Zhu, "Convolutional neural network in intelligent fault diagnosis toward rotatory machinery," *IEEE Access*, vol. 8, pp. 86510–86519, 2020.

[23] C. Q. Yan, *Gas-liquid Two-phase Flow*, Harbin Engineering University Press, Harbin, China, 2009.

[24] T. C. Clayton, *Multiphase Flow Handbook (Mechanical and Aerospace Engineering Series)*, CRC Press, Boca Raton, FL, USA, 2005.

[25] Y. Yang, L. Zhou, and W. Shi, "Interstage difference of pressure pulsation in a three-stage electrical submersible pump," *Journal of Petroleum Science and Engineering*, vol. 196, Article ID 107653, 2020.

[26] Y. Zhang, X. D. Wang, H. Hu, and S. Kang, "Effects of turbulence models on CFD simulations of turbulent jet," *Journal of Propulsion and Technology*, vol. 37, no. 06, pp. 1049–1054, 2016.

[27] T. Lin, Z. C. Zhu, X. J. Li, J. Li, and Y. P. Lin, "Theoretical, experimental, and numerical methods to predict the best efficiency point of centrifugal pump as turbine," *Renewable Energy*, vol. 168, pp. 31–44, 2020.

[28] L. Wang, M. Fan, and X. Y. Zhan, "CFD numerical simulation and model study of anaerobic digestion reactor under gas agitation," *Journal of Agricultural Machinery*, vol. 49, no. 02, pp. 305–312, 2018.

[29] J. Y. Ran, L. Zhang, and M. D. Xin, "Numerical simulation of the flow field of a gradually expanding tangential slot low-pressure swirl nozzle," *Journal of Engineering Thermophysics*, vol. 23, no. 04, pp. 586–588, 2002.

[30] A. Belhadef, A. Vallet, and M. Amielh, "Pressure-swirl atomization: modeling and experimental approaches," *International Journal of Multiphase Flow*, vol. 39, pp. 13–20, 2013.